

Evaluation of Key Geometrical and Mechanical Properties for Remote Laser Welded AC-170PX Aluminium Joints

Abhishek Das, Ian Butterworth, Iain Masters, and David Williams

WMG, The University of Warwick, Coventry, CV4 8GJ, United Kingdom
E-mail: A.Das.I@warwick.ac.uk

Use of lightweight materials to produce automotive body structures is one of the key trends adopted by automotive manufacturers to minimise emission of greenhouse gases, and subsequently, reduction of fuel consumption. Aluminium alloys are one of the promising lightweight materials which are increasingly used for automotive body-in-white structures. Such applications demand both efficient and effective joining/welding methods to produce repeatable, durable and strong joints without significant alteration of material properties. Remote laser welding (RLW) is an emerging joining technology and increasingly being used to produce lightweight joints as it satisfies the demand for high production throughput at low cost. This paper investigates the effects of process parameters when seam tracking remote laser welding is used to create an autogenous fillet edge weld of automotive grade aluminum alloy (AC-170PX) in lap configuration without shielding gas. The effects of laser power and welding speed on the key geometric features are reported together with details of the weld microstructure. Joint strength is evaluated by performing a lap shear test. It is found that the laser power and welding speed have dominant influence on key geometric features and subsequently on the lap shear strength. Relatively larger grain size in the fusion zone reduces the microhardness by up to 20% in comparison with the base material.

DOI: 10.2961/jlmn.2019.01.0001

Keywords: remote laser welding, aluminium welding, seam tracking, fillet edge joint, key geometric features, lap shear strength

1. Introduction

Lightweight materials, especially aluminium alloys, are increasingly being used in automotive, aerospace or rail industries due to their high-strength-to-weight ratio, recyclability and higher crash-energy absorption compared to steel [1, 2]. Especially for automotive applications, aluminium alloys are extensively used for developing structural parts and body-in-white assemblies including outer and inner panels [3, 4]. For outer skin panel application, AA6xxx series alloys (AlMgSi) are exclusively used [5, 6], especially AC-170PX (AA6014) due to excellent formability, hemming performance, very good age hardenability, excellent corrosion resistance and good stability of the mechanical properties during room temperature storage. AC-170PX is predominantly used for critical outer hang-on panels and can also be recommended for demanding inner applications [5].

Making hoods, fenders, door outers or inner panel sub-assemblies using AC-170PX requires joining / welding methods which not only need to provide good joint strength but also to keep parent material properties unaltered [7]. One of the emerging joining technologies, remote laser welding (RLW), has the capability to weld aluminium alloys with increased throughput, reduced energy consumption and lower cost [8, 9]. Unlike conventional laser welding which uses a robot or X-Y coordinate based Cartesian system to manipulate the beam or work piece, remote laser welding uses a comparatively long focusing optic (hence "remote") and scanning mirror(s) to manoeuvre the focused beam over the work piece [10]. As a result, remote laser welding has several advantages over conventional laser

welding including large stand-off distance to minimise the risk of the collision of welding head with the part and fixture, reduction of welding time by combining simultaneous movements of robot position and laser scanner optics (e.g. mirrors), customized welding shapes to increase joint strength on the complex contour of the joining components, and floor space reduction due to fewer joining stations being required [11, 12]. Due to the aforementioned reasons, remote laser welding is gaining significant interest for automotive body-in-white applications. The main two joint configurations (i.e. joint geometries) for RLW in representative top-hat assembly applications are conventional overlap and fillet edge joints, as shown in Fig. 1

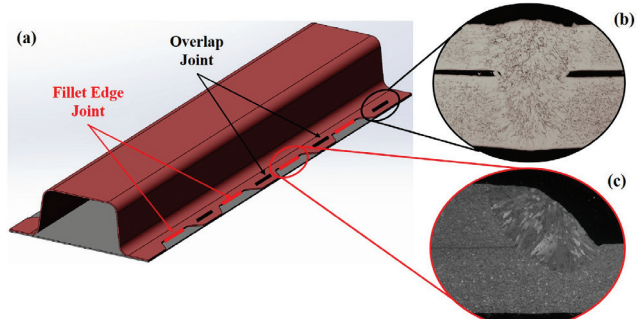


Fig. 1 RLW applications (a) top-hat assembly configuration, (b) overlap joint section, (c) fillet edge joint section.

When joining with RLW process, the fillet edge joint has several advantages over conventional overlap joints including lightweight structure construction due to reduced

flange size, improved quality in terms of fewer pores and less spatter, improved zinc degassing for zinc-coated steel, less fixturing required for part positioning, and removal of the dimpling process required to create part-to-part gap for zinc coated steel [13-15]. These additional benefits from fillet edge weld make it preferred joint configuration for lightweight applications. Additionally, one of the widely used lightweight materials, Al alloys can be benefited from fillet edge weld when producing lightweight body panels for automotive applications. One of the extensively used Al alloys is AC-170PX. Due to the presence of an aluminium oxide layer, enhanced thermal conductivity and high thermal expansion coefficient [16-18], joining aluminium alloys with laser is not trivial. Few investigations are reported on joining of AC-170PX using tactile laser welding where additional filler materials were used to weld, and further, to evaluate weld microstructures and porosity formation [19-21]. Basically, these are near-field laser joining under the shielding gas environment, such as argon gas. On contrary, RLW does not use shielding gas and filler wire which reduces the cost for consumables [12]. However, RLW joining of AC-170PX (Al-Mg-Si) alloy is not reported in literature despite its wide usage within automotive industries.

In this paper, a feasibility study on RLW fillet edge joint is reported in which key geometrical features and mechanical strength of joints are related to the RLW laser power and welding speed.

2. Materials and experiments

This section describes the materials used for this investigation, the experimental set-up and material characterization methods.

2.1 Investigated material properties

The chemical composition and physical properties of the parent material, AC-170PX aluminium alloy, are listed in Table 1.

Table 1 Chemical composition (wt %) and physical properties of AC-170PX (AA6014) used in this study [22, 23]

Alloy Grade : AA6014		
Chemical Composition (wt%)		Physical Properties
Si	0.5-0.7	Density [10^3 kg/m^3] 2.7
Fe	0.35	Young's modulus, E (GPa) 71
Cu	0.25	Shear modulus (GPa) 26
Mn	0.05-0.20	Yield strength (0.2%) [MPa] 90
Mg	0.40-0.8	Tensile Strength, UTS (MPa) 195
Cr	0.10	Poisson's ratio 0.33
Zn	0.10	Strength coefficient, K 407
Ti	0.10	hardening index, n 0.257
Others	0.15	Thermal conductivity [W/m K] 160-190
total max		
Al	Rest	

Two AC-170PX sheets were remote laser welded in a fillet edge configuration. The aluminium sheets were pre-cleaned with acetone to remove lubricant, oil or dirt particles, if any. Therefore, no special surface treatment, such as laser based cleaning, was required to prepare the materials prior to weld.

2.2 Experimental procedures

Remote laser welding was carried out using a Scansonic RLW-A optical head in which optical seam tracking is integrated in the welding head. This facilitates accurate identification of the edge to be joined and focusing the laser on the join patch. A TRUMPF TruDisk 5001 was used as laser power source having maximum power of 5 kW. The laser properties are given in Table 2. Further, the laser head was mounted in KUKA VKRC 150 robot. No filler wire or shield gas were used during the welding as remote laser welding is an autogenous process.

Table 2 Laser unit technical specifications

TRUMPF : TruDisk 5001		
Properties	Unit	Value
Wavelength	nm	1030
Maximum laser power	kW	5
Beam quality	mm*mrad	8
Fiber diameter	μm	200
Nominal focal distance	mm	500
Nominal spot size	μm	580

Two sheets of length = 450 mm and width = 175 mm were used as work pieces to prepare parent assembly for this investigation. The work pieces were assembled by overlapping 25 mm of upper part on the lower part and remote laser welding was carried out in this configuration to produce a fillet edge joint as shown in Fig. 2.

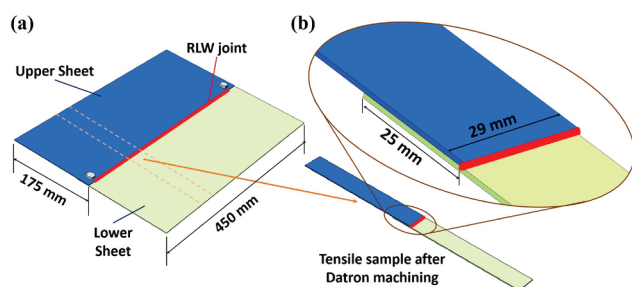


Fig. 2 (a) RLW parent assembly configuration, and (b) tensile sample after Datron machining.

The experimental trials were conducted by varying the laser power and welding speed in order to observe their effects on key geometrical features and shear strength. Initial screening tests were conducted to identify the process parameter levels required to obtain feasible fillet edge welds. Relying on the pilot screening results, laser power was varied from 2.7 kW to 3.1 kW, with an incremental step size of 0.1 kW. Thereafter, the welding speed was increased from 3.0 m/min to 5.0 m/min with an incremental

step size of 0.5 m/min and the welding power was kept at mid value, i.e. 2.9 kW as it produced satisfactory weld. The welding parameters used for experiments are presented in Table 3.

Table 3 Welding parameters for fillet edge joint

Exp Id	Laser Power (kW)	Welding Speed(m/min)
ID 1	2.7	4.0
ID 2	2.8	
ID 3	2.9	
ID 4	3.0	
ID 5	3.1	
ID 6		3.0
ID 7		3.5
ID 8	2.9	4.0
ID 9		4.5
ID 10		5.0

To prepare lap shear and metallographic inspection specimens, the parent assemblies were cut perpendicular to the welding direction. The lap shear specimens were of 29 mm in width [7] as adapted from BS EN ISO 26203-2 [24]. Test samples were prepared using a Datron high speed CNC milling machine. The metallographic samples were mounted in a conductive thermosetting phenolic compression mounting resin. These were ground and polished in four stages. Firstly, grinding was performed using 320 [p400] grit SiC paper until the mounted sample was plane. Secondly, MetaDi supreme diamond suspension solution of 9 μm was used for 5 min, and thereafter, 3 μm MetaDi supreme solution was used for a duration of 4 min as intermediate polishing stages. Finally, a colloidal silica solution of 0.02 – 0.06 μm was used for 3 min to obtain final surface finish. In order to reveal the microstructure of the base material, heat affected zone and fusion zone, the polished samples are anodized in Barker reagent (5 ml Tetrafluoroboric acid, HBF_4 + 100 ml of water) for 120 seconds. The microstructure, fusion geometry and weld surface of the welded samples were examined using an optical surface measurement microscope Alicona IFM G5 3D which is 3D optical non-contact type confocal microscope for surface roughness and topography measurements [25]. For each test condition, three samples were prepared for inspection of the key geometrical features and measurement of the tensile strength in order to obtain consistent and reliable results. Key geometrical features were penetration, leg length and throat thickness as defined in Fig. 3. Microhardness profiles were measured using 300 gf load and a test duration of 10s. Tensile tests (i.e. lap shear tests) were performed using an Instron 5800 test frame with a 100 kN load capacity and cross head speed of 2 mm/min.

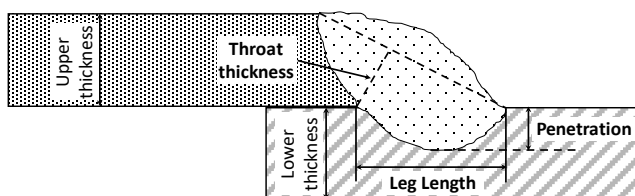


Fig. 3 Typical key geometrical features of RLW fillet edge joint [7, 20].

3. Results and discussions

3.1 Evaluation of key geometrical features

The weld cross sections were examined at relatively low magnification ($\times 5$) using an optical microscope such that the whole joint section could be observed.

Cross-sectional geometry of welded samples

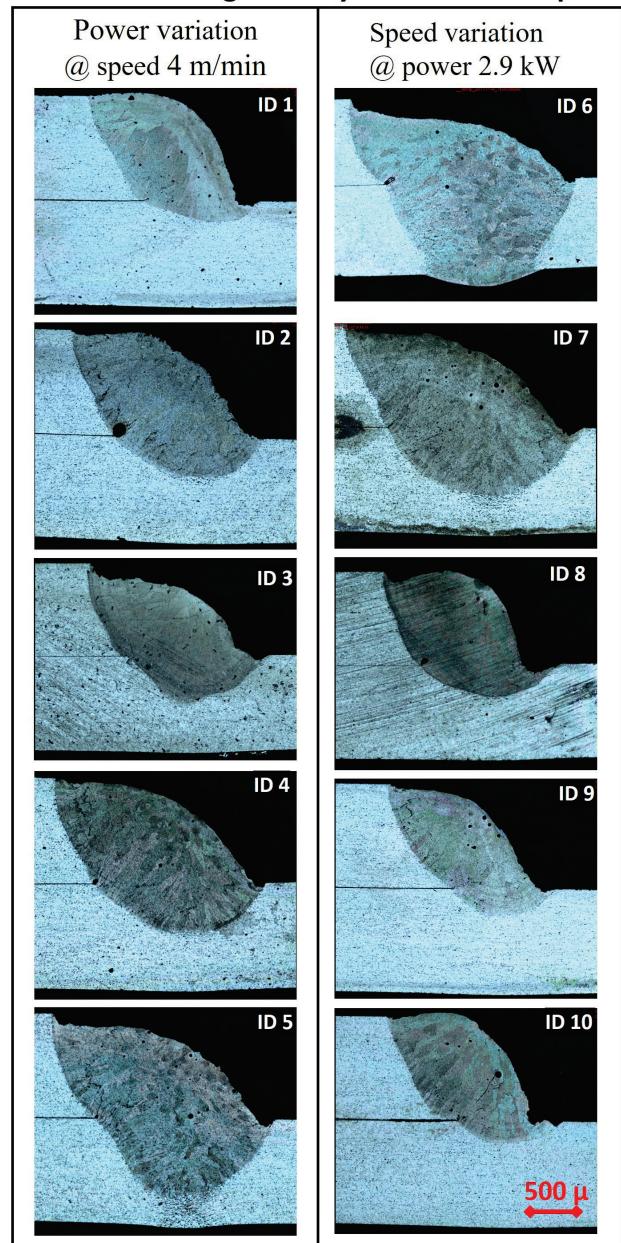


Fig. 4 Cross-section of the fillet edge joints at varying welding parameters as defined in Table 3.

Fig. 4 shows the typical cross section of fillet edge joint at varying laser power and welding speed as described in Table 3. From Fig. 4, it can be seen that the penetration depth increases with laser power when the speed is constant. This is due to the fact that higher power gives higher energy to melt the joining materials. As a consequence, there is an increase in heat input per unit area to melt and fuse materials, as well as slower cooling rate. Similarly, the penetration depth decreases with incremental increase of the welding speed (when the laser power is constant), as the energy input per unit area decreases. At high speed, the joining process had less time to melt and fuse materials, i.e. reduced heat input per unit area which resulted in low penetration depth, also the welds suffered from lack of fusion [7].

After the metallographic inspection, measurement of key geometrical features (i.e. penetration, leg length and throat thickness) are plotted against varying laser power and welding speed as shown in Fig. 5 and Fig. 6, respectively. It can be observed that both laser power and welding speed correlate with the key geometrical features. Laser power exhibits positive correlation with penetration depth, leg length and throat thickness whereas the welding speed shows negative correlation. Heat input per unit area increases with increasing laser power resulting in deeper penetration and wider weld bead which corresponds to greater leg length and throat thickness. In contrast, increasing welding speed reduces the heat input per unit area resulting in negative correlation due to shallower penetration, narrower leg length and thinner throat thickness [7]. It can be noted from Fig. 5 that the penetration, leg length and throat thickness are highest at 3.1 kW laser power; however the weld has bottom surface convexity and penetrates the whole bottom sheet (see Fig. 7). This is not acceptable to industry and often due to aesthetic reason, the bottom surface convexity should be avoided. For example, often the lower side of fillet edge welds in automotive closure panels are visible and bottom surface convexity can cause uneven visual disturbance instead of smooth surface, particularly prominent after the painting. Therefore, it should be avoided. Similarly, welding at 2.9 kW and 3.0 m/in (ID 6) is also not acceptable and in this case, the fusion zone completely penetrates the lower sheet thickness.

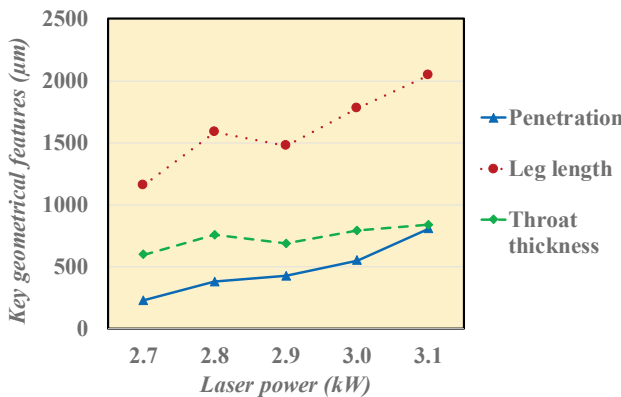


Fig. 5 Key geometrical features at varying laser power.

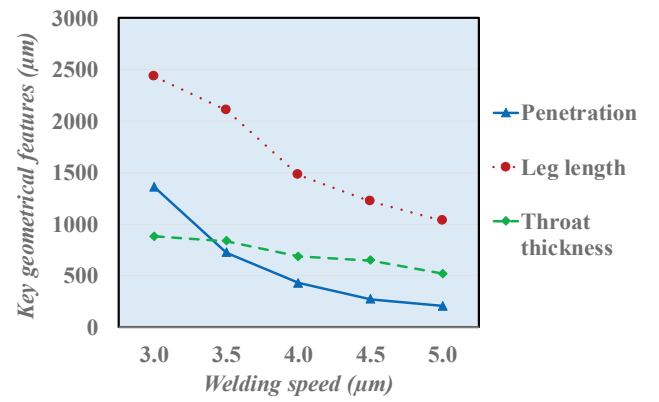


Fig. 6 Key geometrical features at varying welding speed.

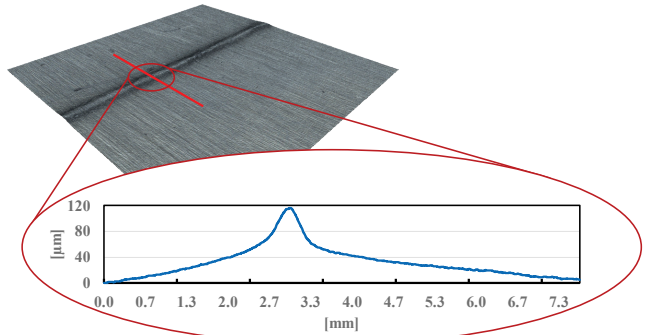


Fig. 7 Bottom surface convexity at 3.1 kW laser power (ID5).

Higher magnification (x50) was used to observe the detailed microstructure of the joint. Fig. 8 shows the detailed microstructure of fillet edge joint prepared using 3.0 kW and 4.0 m/min (ID 4), together with enhanced views of the fusion zone (FZ), heat affected zone (HAZ) and base material (BM). It was found in this study, and also confirmed by Alshaer, et al. [19], that in the AC170-PX base material, dark spots were evenly distributed over the plane aluminum area. Fig. 8 (d) shows a new area from where the columnar growth begins. This area is the transition from base material to fusion zone and also known as HAZ. By moving to the right of the HAZ, fusion zone (FZ) was observed which was full of elongated columnar growth over the grain boundaries. The columnar growth was observed as a result of fast directional solidification at the fusion zone and heat was uniformly conducted away from the fusion zone to the base material [26]. As a result of this directional solidification to the direction of the heat conduction and faster solidification adjacent to the HAZ, elongated columnar grains were observed whereas the top central area of the fusion zone exhibited more equiaxed grains due to slower cooling based solidification. Electron backscatter diffraction (EBSD) image reveals the grain size distribution of base material, narrow heat affected zone and fusion zone (see Fig. 9). It confirms that the average grain size at base material (approx. 34 μm in diameter using linear intercept method) was smaller than the fusion zone where longer columnar growth was observed starting from heat affected zone to fusion zone. It was observed that the heat affected zone width was relatively narrow and ranged in between 10 – 30 μm. At the starting of the fusion zone, the grain size was observed in the range of 300 to 500 μm long as cool-

ing was faster through the base material than compared to the centre of the fusion zone where grain size gradually decreased to around 100 μm .

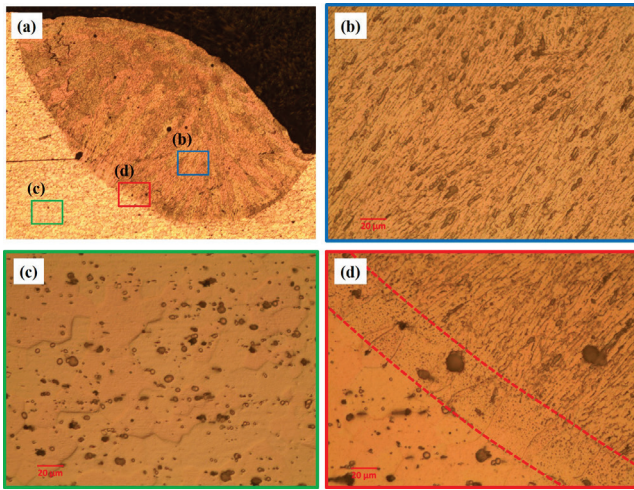


Fig. 8 Microstructure of fillet edge joint at 3.0 kW and 4.0 m/min (a) joint overview, (b) fusion zone (FZ), (c) base material (BM), and (d) heat affected zone (HAZ).

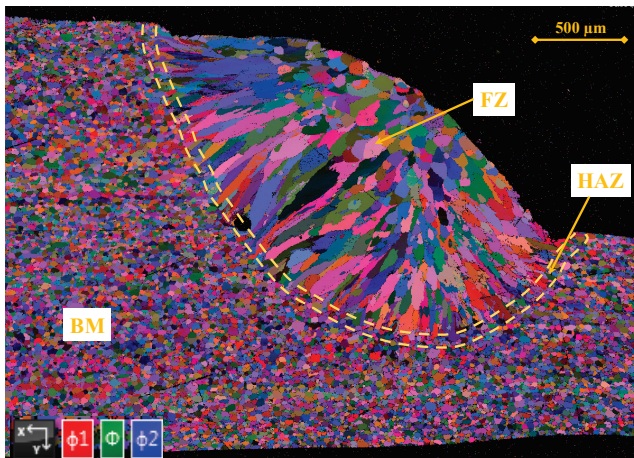


Fig. 9 Electron backscatter diffraction (EBSD) Euler image of fillet edge joint at 3.0 kW and 4.0 m/min showing grain size distribution from BM to FZ.

3.2 Microhardness profile

The measured microhardness profile of the fillet edge joint produced using 3.1 kW laser power and 4.0 m/min welding speed is shown in Fig. 10. For microhardness measurement, anodization step was not performed as only polished surface is better for microhardness measurement. It can be observed that microhardness increases marginally (by up to 5%) in the heat affected zone (HAZ) in comparison with the base material. However, hardness drops were observed in the fusion zone. Similar microhardness behavior was observed by Pakdil, et al. [27] when they investigated AA6056 aluminium alloy using AlSi12 filler wire.

It is widely acknowledged that mechanical properties, including hardness and yield stress of metals and alloys, are influenced by grain size. In general, an increase in hardness and yield strength can be observed when the grain size decreases [28]. In this study, it was observed that average grain size in base material was relatively smaller than the

average grain size in fusion zone and also confirmed by the EBSD analysis. It is worth noting that there is no external material (such as filler wire or powder) was introduced during the welding process and the same parent material was melted and fused together. Therefore, the hardness drop in fusion zone can be attributed to the larger grain size formation and localised hardness due to fusion zone grain orientation. The microhardness decreases by 15% to 20% in the fusion zone.

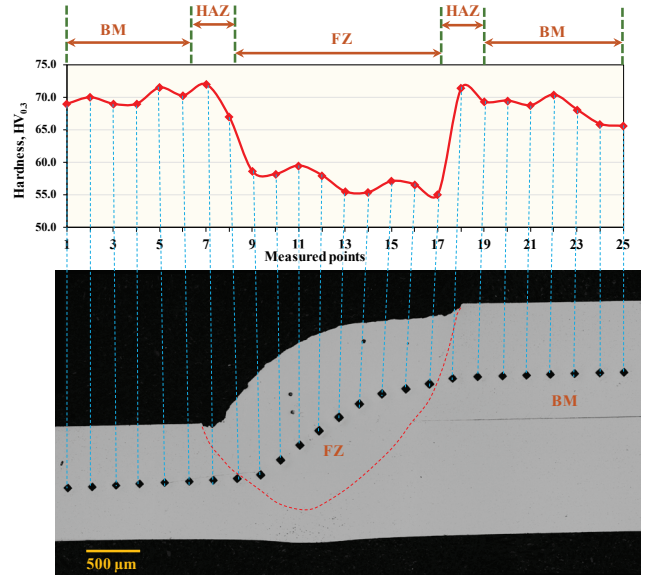


Fig. 10 Microhardness profile of fillet edge joint at 3.1 kW and 4.0 m/min showing BM, HAZ and FZ.

3.3 Evaluation of lap shear strength

The tensile load behaviour was obtained by performing the lap shear tests. The maximum lap shear load at varying laser power and welding are shown in Fig. 11. The maximum loads and corresponding standard errors are given in Table 4. The lap shear strength was increasing with incremental increase of the laser power until 3.0 kW, and then decreased at 3.1 kW which produced over-weld joint with bottom surface convexity. On contrary, maximum lap shear strength was obtained at 4.0 m/min when welding speed was varied from 3.0 m/min to 5.0 m/min. From the welding cross sectional micrographs, it can be observed that full penetration was achieved when welding at lower speed (i.e. 3 m/min). This is due to the fact that lower speed leads to an increase in heat input which results in full penetration and makes the weld weaker. However, at higher welding speed, there is substantial reduction in heat input and an increase in cooling rate which resulting in shallower penetration, narrower leg length and consequently, reduced tensile strength. At lower welding speed, even though it produced over-welds, the joint strength was higher since the fusion zone had overall good contact area with the base materials. In contrast, the under-weld joints at higher welding speed yielded at much lower strength due to low penetration, and subsequently, low contact area with the base materials. As a result, the rate of change in lap shear load was low in between 3.0 m/min to 4.0 m/min and decreased rapidly from 4.0 m/min to 5.0 m/min. A preferred penetration depth was obtained at 4 m/min and 2.9 kW (ID 8)

where penetration depth was 426 μm (i.e. less than 50% of lower sheet thickness) and maximum tensile load was obtained. It is worth noting that the rate of change in lap shear variation is comparatively lower for the laser power variation than the welding speed. This is due to the fact that the rate of change in heat input per unit area was lower for laser power variation than the welding speed variation. For example, the rate of change in heat input per unit area was approximately 3.5% for stepwise increase in laser power whereas it was 10-14% for the changes in welding speed.

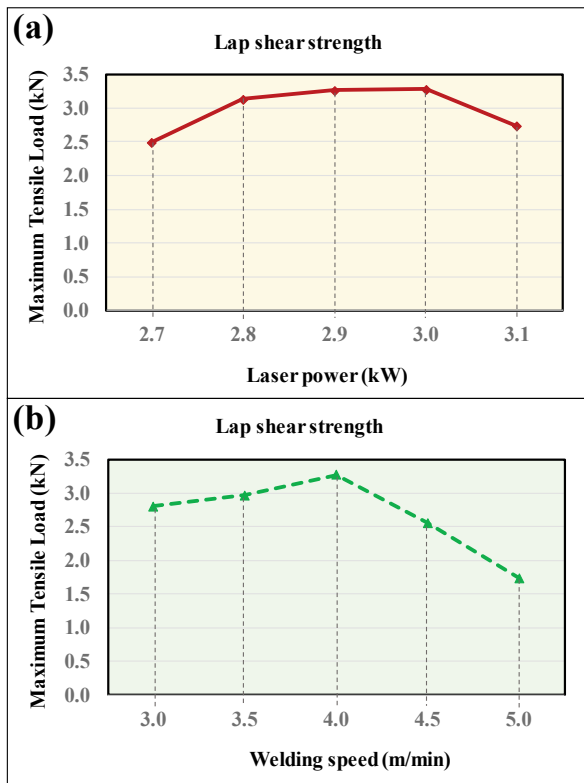


Fig. 11 Maximum tensile load from lap shear tests at varying (a) laser power (ID 1-5), and (b) welding speed (ID 6-10).

Table 4 Maximum loads and corresponding standard errors

Exp Id	Maximum load [kN]	Standard error
power variation	ID 1 2.50	0.010
	ID 2 3.13	0.035
	ID 3 3.27	0.021
	ID 4 3.28	0.012
	ID 5 2.74	0.020
Welding speed variation	ID 6 2.80	0.074
	ID 7 2.96	0.072
	ID 8 3.27	0.021
	ID 9 2.55	0.019
ID 10	1.73	0.020

4. Conclusions

This paper has shown the feasibility of remote laser welding application to produce fillet edge joint with a widely used aluminium alloy, AC-170PX (AA6014). The effects of laser power and welding speed on key geometrical features of the weld and lap shear strength have been reported with detailed microstructure including BM, HAZ and FZ. This paper has identified and explored the following areas:

- The laser power and welding speed have substantial influence on the key geometrical features, such as penetration depth, leg length and throat thickness. Increase in laser power leads to more heat input to produce deeper penetration and wider leg length. The welding speed has negative correlation with key geometrical features as higher welding speed leads to less energy input and faster cooling of fusion zone.
- When laser power was increased from 2.7 kW to 3.1 kW (ID 1 to ID 5), penetration depth was gradually increased up to 3.5 times and reached near full penetration with bottom surface convexity.
- Full penetration with bottom surface convexity was observed at 3.0 m/min and the measured value of the penetration depth was 1358 μm which was greater than the thickness of the bottom surface. The penetration depth decreases with increase of welding speed and was 203 μm at 5.0 m/min. similar decreasing trend was observed for leg length and throat thickness.
- It was observed that preferred laser power and welding speed resulted in good quality joints with higher lap shear strength. In this experimental feasibility study, maximum tensile load was observed as 3.28 kN at 3.0 kW and 4 m/min.
- EBSM analysis for grain size mapping confirmed that larger grain distribution in the fusion zone compared to base material.
- Microhardness was decreased by about 10-15 HV_{0.3} when moving from the base material to fusion zone. The hardness drop in fusion zone can be attributed to the larger grain size formation.

Acknowledgments

This research is partially supported by Scansonic IPT GmbH with laser experimental trials. Characterization and testing were provided by the WMG Centre High Value Manufacturing (HVM) Catapult at The University of Warwick.

References

- [1] R. Smerd, S. Winkler, C. Salisbury, M. Worswick, D. Lloyd, and M. Finn: Int. J. Impact Engg., 32, (2005) 541.
- [2] M. Allen, M. Oliveira, S. Hazra, O. Adetoro, A. Das, and R. Cardoso: J. Phys.: Conf. Series, 734, (2016) 022002.
- [3] A. Das, P. Franciosa, D. Williams, and D. Ceglarek: Proc. CIRP, 41, (2016) 1072.
- [4] A. Das, P. Franciosa, A. Pesce, and S. Gerbino: Int. J. Engg Sci. Tech., 9, (2017) 117.

- [5] M. Bloeck: *Adv. Mat. Autom. Engg.*, (2012) 85.
- [6] J. Hirsch: *Trans. Nonfer. Met. Soc. China*, 24, (2014) 1995.
- [7] A. Das, I. Butterworth, I. Masters, and D. Williams: *Mat. Charac.*, 145, (2018) 697.
- [8] A. Fysikopoulos, G. Pastras, J. Stavridis, P. Stavropoulos, and G. Chryssolouris: *Proc. CIRP*, 41, (2016) 969.
- [9] A. Das, P. Franciosa, and D. Ceglarek: *Proc. Manufac.*, 1, (2015) 157.
- [10] K. Mori, T. Tarui, T. Hasegawa, and N. Yoshikawa: *Weld. Int.*, 24, (2010) 758.
- [11] G. Reinhart, U. Munzert, and W. Vogl: *CIRP Annals – Manufac. Tech.*, 57, (2008) 37.
- [12] A. Das, “Shape variation modelling, analysis and statistical control for assembly system with compliant parts”, PhD Thesis, WMG, Uni. of Warwick, 2016.
- [13] P. Fixemer, F. Albert, P. Sievi, and T. Graham: *Laser Technik J.*, 12, (2015) 38.
- [14] D. Colombo and B. Previtali: *Int. J. Adv. Manufac. Tech.*, 72, (2014) 653.
- [15] C. Roos and M. Schmidt: *Phys. Proc.*, 56, (2014) 535.
- [16] A. El-Batahgy and M. Kutsuna: *Adv. Mat. Sci. Engg.*, 2009.
- [17] A. Das, D. Li, D. Williams, and D. Greenwood: *World Elec. Vehc. J.*, 9, (2018) 22.
- [18] L. Quintino, R. Miranda, U. Dilthey, D. Iordachescu, M. Banasik, and S. Stano: *Struc. Connec. Lightweight Met. Struc.*, (2012) 33.
- [19] A. Alshaer, L. Li, and A. Mistry: *J. Manufac. Sci. Engg.*, 137, (2015) 021011.
- [20] A. W. Alshaer, L. Li, and A. Mistry: *Proc. Inst. Mech. Engrs., Part B: J. Engg. Manuf.*, 231, (2015) 994.
- [21] L. A. Pinto, L. Quintino, R. M. Miranda, and P. Carr: *Weld. World*, 54, (2010) R333.
- [22] A. W. Alshaer, L. Li, and A. Mistry: *Optics & Laser Tech.*, 64, (2014) 162.
- [23] S. Sun and D. E: *Mat. & Design*, 93, (2016) 118.
- [24] BS EN ISO 26203-2: BSI Standards Publication, 2011.
- [25] <https://www.alicona.com/products/infinitefocus/>
- [26] M. Zhang, G. Chen, Y. Zhou, and S. Liao: *Mat. & Design*, 53, (2014) 568.
- [27] M. Pakdil, G. Çam, M. Koçak, and S. Erim: *Mat. Sci. Engg. A*, 5284, (2011) 7350.
- [28] Y. Y. Lim and M. M. Chaudhri: *Philos. Magz. A*, 82, (2002) 2071.

(Received: April 22, 2018, Accepted: December 27, 2018)